# Coexisting Glassy Phases with Different **Compositions in NFA-Based Bulk** Heterojunctions

Oded Nahor, Aditi Khirbat, Sebastian Alexander Schneider, Michael F. Toney, Natalie Stingelin,\* and Gitti L. Frey\*



Downloaded via GEORGIA INST OF TECHNOLOGY on November 13, 2023 at 15:53:45 (UTC). See https://pubs.acs.org/sharingguidelines for options on how to legitimately share published articles.

Cite This: ACS Materials Lett. 2022, 4, 2125-2133

MATERIALS

www.acsmaterialsletters.org



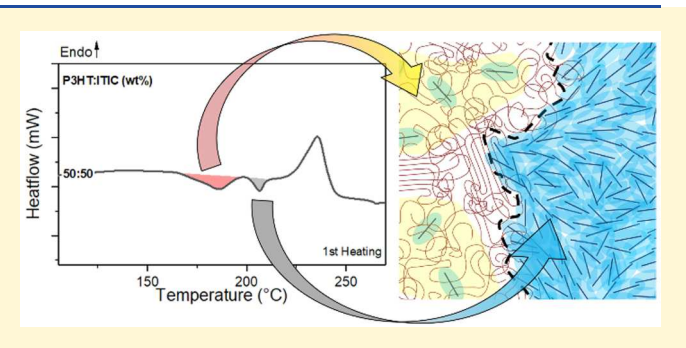
**ACCESS** I

Metrics & More

Article Recommendations

Supporting Information

ABSTRACT: Organic solar cell (OSC) bulk heterojunctions (BHJ) typically feature a rich phase morphology with the phase composition and distribution significantly affecting processes such as charge generation, recombination and extraction, and in turn, device performance. While fullerene-based BHJs are relatively well understood structurally, especially when blends with a flexible-chain donor are employed, donor: non-fullerene acceptor (NFA) blends are more challenging to elucidate. The reason is that NFAs often display different polymorphs; moreover, their glassy states can be complex. Focusing on blends of the widely investigated donor polymer, poly(3-



hexylthiophene-2,5-diyl) (P3HT), and the prototype NFA, 3,9-bis(2-methylene-(3-(1,1-dicyanomethylene)-indanone))-5,5,11,11-tetrakis(4-hexylphenyl)-dithieno[2,3-d:2',3'-d']-s-indaceno[1,2-b:5,6-b']dithiophene (ITIC), we reveal here the coexistence of two glassy phases: a molecularly intermixed and an ITIC-rich one. In P3HT-rich blends, both glassy phases are present as nanosized domains, evenly distributed in the BHJ, as visualized via vapor phase infiltration (VPI) "staining". In contrast, the 1:1 (by weight) and NFA-rich blends show clear, lateral phase separation between large (>500 nm) domains of the glassy phases and thinner polymer-rich domains that are unaffected by annealing. Our observations help to explain earlier P3HT: ITIC device studies; and also highlight the complexity of NFA-based BHJs, emphasizing the need for a deeper understanding of the phase behavior of such systems.

Tolution processed organic solar cells (OSC) promise low-cost, flexible, and lightweight alternatives to inorganic photovoltaic technologies, 1-3 with power conversion efficiencies (PCE) having evolved dramatically from about 9% in 2012<sup>4</sup> to over 18% today.<sup>5</sup> This significant improvement is predominantly due to the advancement of small-molecule non-fullerene acceptors (NFAs) that, in contrast to fullerenes widely used prior to 2016, are of a narrow band gap and contribute to light absorption.<sup>6</sup> NFAs also differ from fullerenes with respect to the molecular packing motifs they can feature. The reason is that, contrary to fullerenes, NFAs are not spherical, and strong intermolecular interactions may form between NFA molecules that can lead to aggregation or polymorph formation. 8,9 Their often complex chemical structure can limit molecular ordering, which can result in vitrification.<sup>8,9</sup> As a consequence, new understanding and broadly applicable design rules are needed to enable the prediction of phase morphologies of NFA-based OSC blends toward optimized photovoltaic device performance.

In order to begin our discussion, we recall that OSC bulk heterojunctions (BHJs) can often be composed of a complex mixture of phases. In the most efficient fullerene-based OSCs, the BHJ morphology can be described by the presence of three types of phases, especially if a flexible-chain donor polymer is used. These include a donor-rich phase, an acceptor-rich phase, and an intermixed phase composed of the donor and the acceptor. 10,11 Although the phase composition, 11-13 relative donor/acceptor fractions, 14,15 size, 11,16 and, e.g., lateral and vertical phase distribution<sup>17–19</sup> differ from system to system, some general guidelines have been advanced for such fullerenebased OSCs. It has, for instance, been shown that the

Received: July 11, 2022 Accepted: September 21, 2022 Published: September 28, 2022





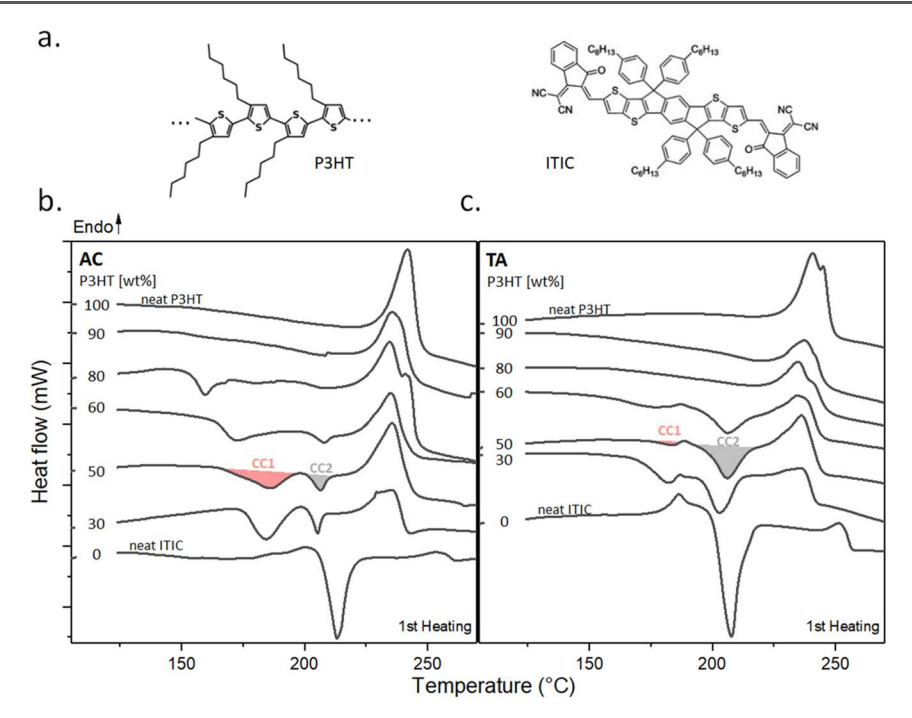


Figure 1. (a) Chemical structures of P3HT and ITIC. (b, c) DSC thermograms of P3HT: ITIC blends: (b) as-cast blends and (c) after thermal annealing at 150 °C for 10 min.

composition and distribution of the often vitrified, intermixed donor: acceptor domains affect important processes, such as charge generation and charge recombination. 10,20,21 The amount of the intermixed phase that may form in fullerenebased BHJs was thereby found to be dictated by donor: acceptor interactions,<sup>21</sup> polymer molecular weight,<sup>20</sup> blend composition,<sup>20</sup> miscibility<sup>22</sup> and processing conditions—i.e., kinetic and thermodynamic factors. During film formation, precipitation, crystallization, and demixing processes compete with nonequilibrium quenching effects, e.g., vitrification, which suppresses polymer crystallization and leads to amorphous solid solutions.<sup>22</sup> Such intermixed glasses can evolve over time, which occurs more rapidly at elevated temperatures, e.g., when the system is heated above its glass transition temperature  $(T_a)^{\frac{4}{5},23,24}$  but this can be limited by restricting molecular diffusion/mass transport via introduction of cross-links between the donor and acceptor,<sup>25</sup> use of donor polymers of high molecular weight<sup>25</sup> or selection of donor and/or acceptors with a high  $T_{\rm g}$ .  $^{26,27}$ 

The structure-property-performance relations developed for fullerene-based systems may not be applicable to the NFAbased systems, despite their similar photophysical behavior, their comparable low dielectric constants and their relatively limited charge-carrier mobilities.<sup>6,28</sup> Therefore, one cannot build on the knowledge and expertise gained for fullerenebased devices for developing understanding of NFA-based systems. To mitigate the laborious trial-and-error efforts invested in the design and processing of high performing NFA-based OSCs, it is necessary to investigate and disentangle the complex interactions and phases that are present and dominate the NFA-based systems. Here, we selected the prototype indacenodithienothiophene-based NFA, 3,9-bis(2methylene-(3-(1,1-dicyanomethylene)-indanone))-5,5,11,11tetrakis(4-hexylphenyl)-dithieno[2,3-d:2',3'-d']-s-indaceno-[1,2-b:5,6-b']dithiophene (ITIC),<sup>29</sup> as a model acceptor together with poly(3-hexylthiophene-2,5-diyl) (P3HT) (Figure 1a), a materials combination that each has been shown to form glassy intermixed phases in BHJs. 8,22 While this system exhibits a very low PCE of about 1.25%,30 the thermal and structural behavior of the neat materials have been widely investigated,9,31-34 which provides the knowledge for us to understand the phase behavior of P3HT: ITIC BHJs and will yield general insights on NFA-based systems.

We start our investigation with the thermal analysis of ascast (AC) P3HT: ITIC blends, along with the neat components as reference, using differential scanning calorimetry (DSC). The first heating thermograms of AC neat P3HT, neat ITIC, and P3HT: ITIC blends of different compositions, deposited from chlorobenzene are presented in Figure 1b (concentrations ranged from 20 mg/mL for the neat solutions to 40 mg/mL for the 1:1 solution, as detailed in the Supporting Information (SI)). Upon heating (20 °C/min), AC neat P3HT shows a clear melting endotherm (T<sub>m</sub>) at 240 °C (taken from the peak temperature), in agreement with literature.<sup>35</sup> For neat ITIC, we observe a dominant exotherm centered around 210 °C and a weak endotherm around 250 °C. For the P3HT: ITIC blends, the endotherm due to melting of crystalline P3HT moieties is visible in the thermograms of all blends. ITIC-rich blends, in addition, feature two prominent exotherms around 180 °C (CC1) and 210 °C (CC2). These may be assigned to cold-crystallization processes resulting from the fact that solution-blending P3HT and ITIC leads to films of low molecular order, i.e., partial vitrification occurs during solidification because crystallization of one (or both) blend component(s) is hindered by presence of the other<sup>22</sup>—a view that is supported by GIWAXS data (vide infra). Notably, it is likely that the solution processing of this system caused it to pass through the Berghmans point as the phase separation of the system was hindered and vitrified phases were obtained.<sup>36</sup>

To obtain more quantitative insight on the possible partial vitrification from solution of P3HT: ITIC blends and how they cold-crystallize when they are heated in the solid-state, we

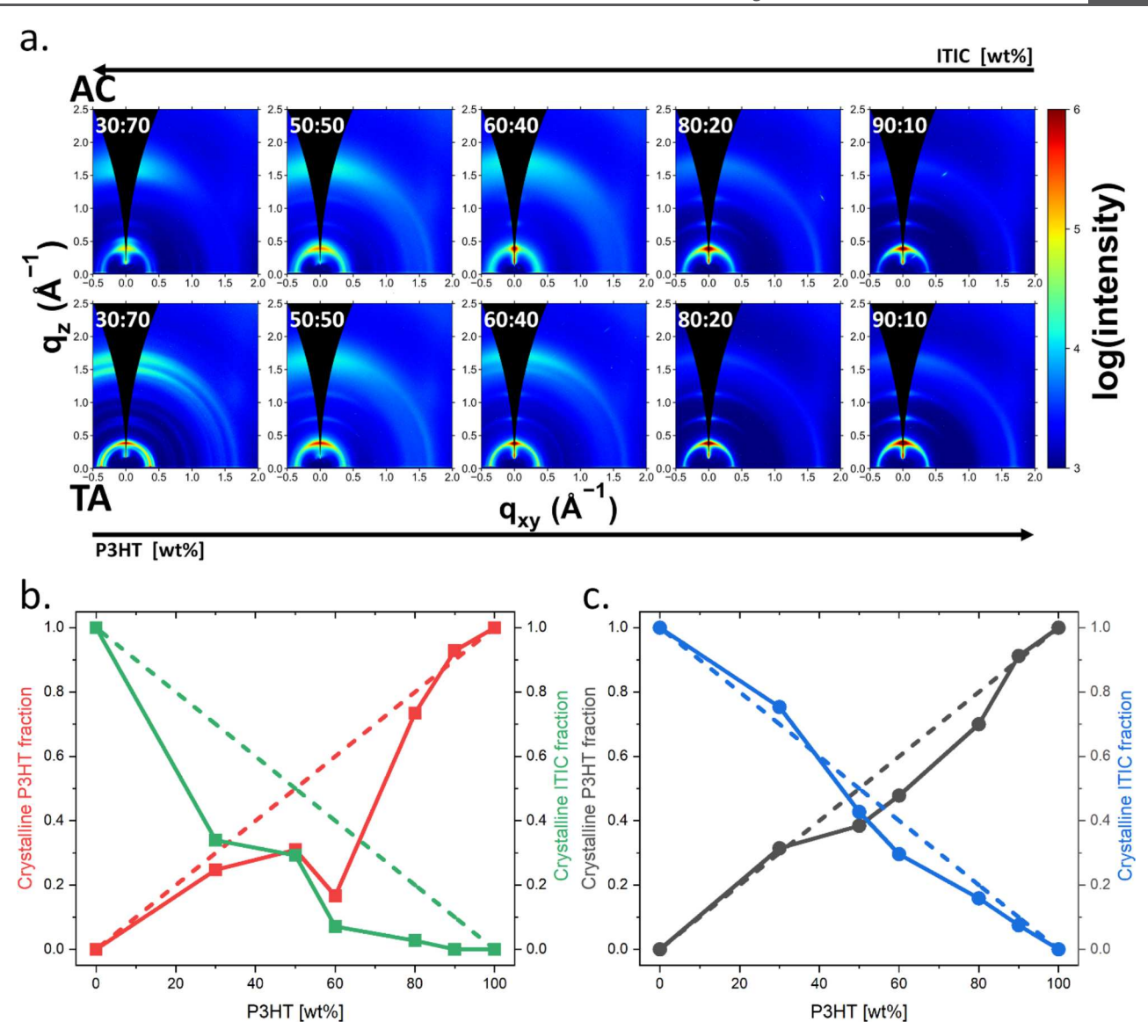


Figure 2. (a) 2D GIWAXS patterns of P3HT: ITIC bend films (blend ratio given in wt %). Top row: Patterns of as cast fims (AC). Bottom row: Same films after thermal annealing (TA). (b, c) Crystalline fractions of P3HT (red and black) and ITIC (green and blue) for AC P3HT: ITIC films (b) and TA blend films (c). The dashed lines show the fraction that can be calculated for a hypothetical, immiscible system where the two components can crystallize essentially freely, using the linear combination of the scattering intensities of neat P3HT and ITIC films, weighted by the respective mass fractions of the different blends. The continuous lines are the actual values calculated from the GIWAXS patterns measured for AC and TA blend films. A crystalline fraction below the dashed line indicates that blending the materials suppresses crystallization and the materials are more amorphous in the blend as compared to the neat films.

performed grazing-incidence wide-angle X-ray (GIWAXS) measurements (Figure 2a and Figure S1). We use (h00) and (0k0) to denote the lamellar and  $\pi$ – $\pi$  stacking planes of P3HT and ITIC, respectively, while (00l) is along the long molecular axis. The AC ITIC films (Figure S1, top left) show weak and broad (100) and (001) peaks in plane, and the (010) out-of-plane peaks, indexed following Mai et al.<sup>37</sup> and indicating predominant face-on orientation of low-ordered ITIC crystallites. The pattern of the AC P3HT film (Figure S1, top right) exhibits up to three orders of the lamellar stacking peak (h00) in the out-of-plane direction with the lowest order, (100), at  $q_z = 0.387$  Å<sup>-1</sup> (d(100) = 16.2 Å), consistent with previous reports. <sup>38,39</sup> Combined with the  $\pi$ – $\pi$  stacking peak (010) in the in-plane direction at  $q_{xy} = 1.68$  Å<sup>-1</sup> (d(010) = 3.74 Å), the 2D scattering patterns, thus, indicate predominantly edge-on orientation of P3HT crystallites.

The orientation of P3HT crystallites remains predominantly edge-on throughout the series of blend films with different P3HT content (Figure 2a). Moreover, with increasing P3HT fraction, we observe a qualitative decrease in the intensity of the ITIC GIWAXS diffraction, while those of P3HT become more intense. The effect of blending on the degree of crystallinity of the blend components can be quantified by calculating the crystalline fractions of P3HT and ITIC in the AC blend films. We tracked for this purpose the relative degree of crystallinity (rDoC) of both components separately across all blend ratios. 40,41 Specifically, we fitted the P3HT (200) and the ITIC (200) peaks to quantify the scattering of crystalline P3HT and ITIC. We chose these peaks because they provide the least overlap with other peaks in the scattering patterns presented in Figure 2a. The resulting peak areas for P3HT and ITIC were then normalized relative to the peak area of neat

P3HT (100 wt % P3HT) and ITIC (0 wt % P3HT), yielding the relative crystalline fraction of both materials for the varying blend ratios  $^{41}$  (see SI).

The solid lines in Figure 2b show the crystalline fraction of P3HT (red) and ITIC (green) calculated from the GIWAXS patterns of the different blends displayed in Figure 2a, while the corresponding dashed lines describe the crystalline fractions for a hypothetical, fully immiscible blend, where both materials would be able to crystallize essentially unhindered; i.e., a scenario where the blend components crystallize as in the neat materials. Accordingly, the expected scattering intensities of the P3HT and ITIC fractions in such hypothetical immiscible blends can be calculated by weighting the scattering intensity of neat P3HT and ITIC films to the respective mass fractions of the two components. A crystalline fraction below this dashed line, as a consequence, indicates that blending suppresses crystallization of the specific component, leading to a higher molecular disorder in the blend as compared to the neat films. A positive deviation, on the other hand, suggests that blending of the materials promotes the crystallization of one or both components.

Detailed information can be obtained from such an analysis. For instance, we observe that P3HT in the AC 90:10 P3HT: ITIC (by weight) blend films follows essentially the behavior of immiscible systems, indicating that the presence of 10 wt % ITIC does not affect P3HT crystallization. However, increasing the ITIC content above 10 wt % induces a pronounced deviation from the value that can be calculated for the crystalline P3HT fraction in an immiscible blend, with the strongest divergence found for the AC 60: 40 P3HT: ITIC blend films (red squares in Figure 2b). The crystalline P3HT fraction recovers for the 50: 50 P3HT: ITIC blend, adopting a value closer to the ones calculated for immiscible blends, and it fully returns to values that immiscible blends would show at higher ITIC content. We conclude that the degree of crystallinity of P3HT is reduced in blends with ITIC (especially at compositions around 50% P3HT). This picture is supported by a systematic decrease of the coherence length  $(L_C)$  of P3HT crystallites as a function of ITIC addition in the different AC blends films (see Figure S2 and analysis in SI section). Notably, the ITIC crystalline fraction in all blends deviates significantly from the value that immiscible binaries would adopt.

We infer from these observations that the two components in the AC blend films initially are at least partially vitrified, in agreement with the fact that we see exotherms in our DSC heating thermograms that suggest that as cast films are of low (or lower) molecular order. Intriguing is that, in DSC, we observe two distinct exotherms upon heating the blends. We hypothesize that we have different types of amorphous phases present in the P3HT: ITIC—a glassy intermixed phase formed because of blending (and crystallizing in the temperature region indicated with CC1), and an ITIC-rich glass (coldcrystallizing in the CC2-regime). This picture is supported by the fact that the CC1 peak temperature, measured in DSC, shifts to lower temperatures in blends of higher P3HT content (Figure S3a, solid pink lines), which would be expected for an intermixed phase of varying composition, where the phase transition (here CC) will be dependent on the amount of P3HT in this phase. In contrast, CC2 is recorded in essentially the same temperature range across the different blend ratios (dashed pink lines in Figure S3a), suggesting that this phase's composition does not vary much across the different blends.

We, thus, infer that this exotherm results from the cold crystallization of relatively phase-pure, ITIC-rich amorphous domains, consistent with the low rDoC for ITIC at high P3HT concentrations. This means that P3HT: ITIC BHJs can be composed of two different glassy populations that coexist: an amorphous intermixed phase comprising P3HT and ITIC and crystallizing at CC1, and an amorphous ITIC-rich phase that begins to molecularly order in the CC2 temperature regime. This is in strong contrast to fullerene-based BHJs that typically are composed of one type of amorphous phase, the intermixed phase comprised of the donor and the acceptor. <sup>22,42</sup>

This hypothesis can be corroborated when analyzing thermally annealed (TA) films and compare them with the data obtained for as-cast structures. We selected as annealing temperature 150 °C, which is at the onset (upon heating) for the CC1 process for most blend films (see Figure 1b). The enthalpies  $(\Delta H)$  of both CC processes in the AC and TA blends were deduced from the thermograms displayed in Figures 1b and c and compared in Figure S3b. We find that annealing significantly reduces the enthalpy  $(\Delta H)$  of the CC1 exotherm, while notably increasing for CC2, to the extent that in the AC blends  $\Delta H_{\rm CC1}$  >  $\Delta H_{\rm CC2}$ , while in the TA samples  $\Delta H_{\rm CC1} < \Delta H_{\rm CC2}$ . These observations indicate that annealing at 150 °C increases the population of the glassy ITIC-rich phase at the expense of the intermixed amorphous phase. The dissolution of the intermixed phase during annealing is also reflected in an increase of the melting enthalpy  $\Delta H_{\rm m}$  of P3HT (Figure S3b) and the nearly full recovery of the crystalline fractions obtained from GIWAXS to values calculated for hypothetical immiscible blends (Figure 2c). The slight deviation from the values that immiscible systems would adopt at compositions of around 50-70% P3HT may be attributed to some remaining glassy intermixed domains. We, therefore, conclude that upon annealing, the amorphous intermixed domains phase-separate into P3HT- and ITICrich regions. The fact that  $\Delta H_{CC2}$  increases in the annealed films compared to AC structures, suggests that some of the phase-separated fraction of this ITIC remains amorphous, only ordering at CC2.

In order to visualize the complex phase morphology of the P3HT: ITIC binaries, we exposed the blend structures to gaseous metal oxide precursors that diffuse into the films and in situ convert to an inorganic product. Precursor diffusion is, typically, permitted in domains with free volume, such as amorphous polymer regions and permeable glassy (intermixed) domains, but it is restricted in <u>dense</u> glassy domains produced by molecularly intermixed phases. Such vapor phase infiltration (VPI) "staining" can complement the above X-ray and DSC data, as the heavy atoms' preferential interdiffusion and conversion in certain phases offers high contrast when analyzing the resulting samples by scanning electron microscopy (SEM). Specifically, Z (atomic number)-contrast in cross section HRSEM can be used to map the distribution of inorganic-free and "stained" domains.

We started with exposing AC and TA neat P3HT and ITIC films to a VPI sequence of tetrakis(dimethylamido)hafnium (TDAHf) and water, 47,48 which led to metal oxide precursor diffusion and HfO<sub>2</sub> deposition inside amorphous domains in the polymer film, but not in the dense ITIC film, as can be clearly observed in the micrographs presented in Figure S4. Upon blending, the phase morphology of AC P3HT-rich blends (90 and 80 wt % P3HT) generally stays unchanged compared to that of neat P3HT, with HfO<sub>2</sub> particles being

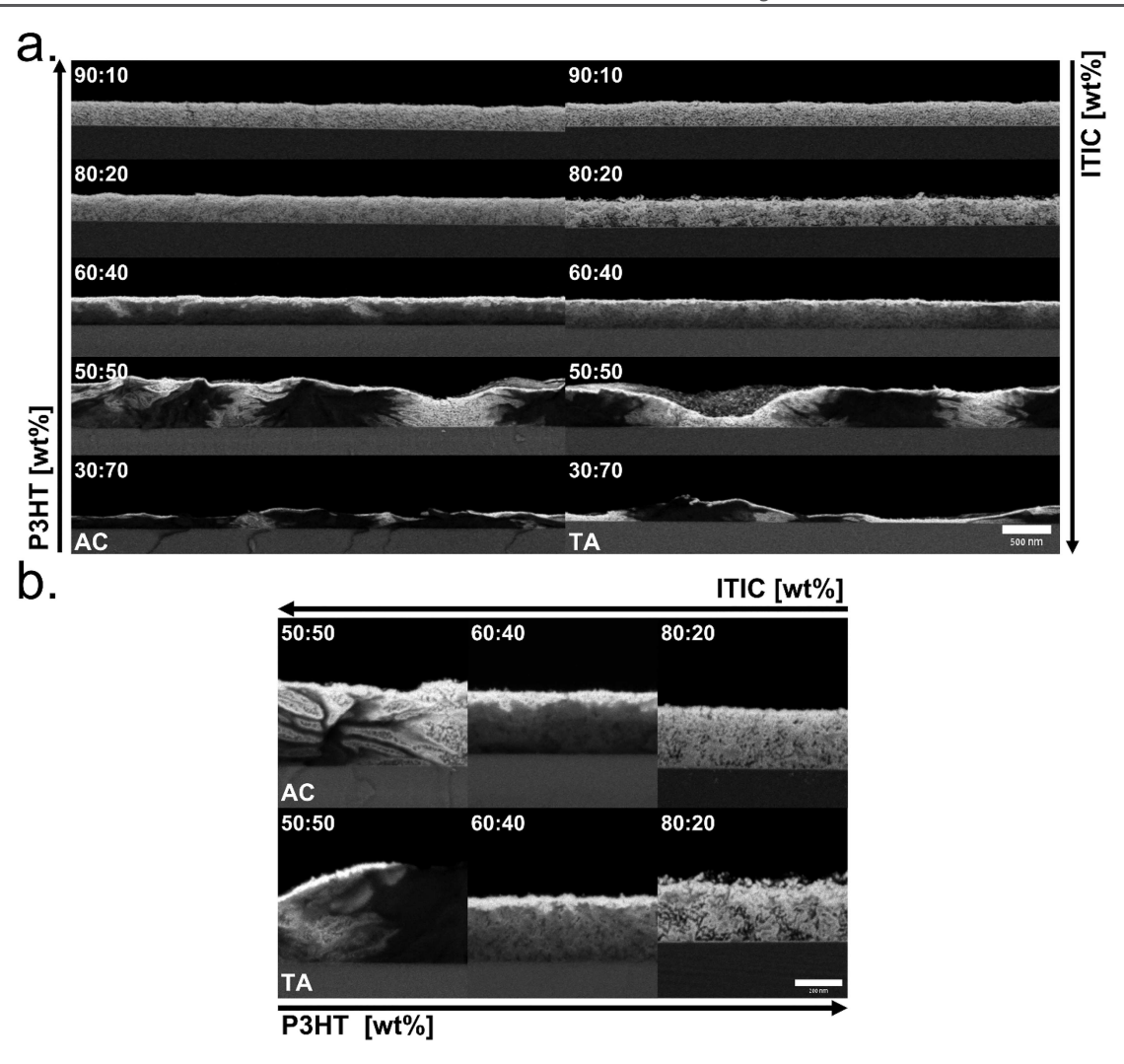


Figure 3. (a) Cross section HRSEM BSE micrographs of AC (left column) and TA (right column) P3HT: ITIC blend after a TDAHf/H<sub>2</sub>O VPI process showing selective deposition of HfO<sub>2</sub> in the P3HT-rich domains (bright contrast). In contrast, the mixed glassy phase domains and ITIC-rich domains inhibit HfO<sub>2</sub> deposition and, thus, are characterized by dark contrast. The selective "staining" of P3HT-rich domains by HfO<sub>2</sub> in the VPI process effectively maps the phase separation as well as the size- and spatial distribution of the domains in P3HT: ITIC blend films. The scale bar for all micrographs is 500 nm. (b) High-magnification cross section HRSEM BSE micrographs of the AC (top) and TA (bottom) P3HT: ITIC blends after the TDAHf/H<sub>2</sub>O VPI process showing P3HT-rich domains (bright contrast) and mixed glassy phase and ITIC-rich domains (dark contrast). The scale bar for all micrographs is 200 nm.

evenly distributed in the films (Figure 3a). This suggests that in such structures, the glassy intermixed P3HT: ITIC phase present in these systems is permeable and homogeneously dispersed in small domains throughout the films. Note that generally, the VPI methodology cannot distinguish between the two glassy phases, i.e. the intermixed P3HT: ITIC phase vs the ITIC-rich amorphous phase, as they both seem to resist the diffusion of the precursors. However, the density of the glassy intermixed P3HT: ITIC phase can vary with ITIC content so that at low ITIC content (80: 20) this phase might also be stained. Moreover, annealing these P3HT-rich films induces ITIC aggregation, as identified by the GIWAX analysis (Figure 2c), and via VPI as dark domains that remain small in size and are well dispersed with a minor tendency toward separation to the bottom interface, as can be observed in HRSEM images. These aggregated ITIC domains thereby seem to be somewhat larger than the glassy domains (see Figure 3b for an example of a high magnification image of TA 80: 20 P3HT: ITIC film). Increasing the ITIC content further to 40 wt % ITIC (P3HT 60 wt %) leads in AC films to dense glassy domains vertically

separating toward the bottom substrate, evident from the gradient of HfO<sub>2</sub> deposition throughout the film (high magnification image in Figure 3b). Annealing the film induces some ITIC aggregation but the molecular ordering process is limited by the high ITIC content, leading to a BHJ with a polymer-rich top phase, domains of the intermixed and ITIC-rich glassy phases dispersed in the film, and ITIC crystalline domains at the bottom. It is important to note that this phase morphology could be beneficial for OSCs with bottom, electron-collecting cathodes.

In strong contrast to these vertically separated structures, for AC 50:50 P3HT: ITIC films, a noticeable <u>lateral</u> phase separation is observed, with very large (>500 nm) dense domains (dark regions in HRSEM image) being separated by thinner polymer-rich domains (bright in HRSEM image). Similar observations can be made for AC 30:70 P3HT: ITIC blends, but the polymer-rich domains seem thinner based on the brightness contrast we observe. Moreover, annealing does not drastically affect the overall morphology, but it blurs the boundaries between the P3HT- and ITIC-rich domains. The

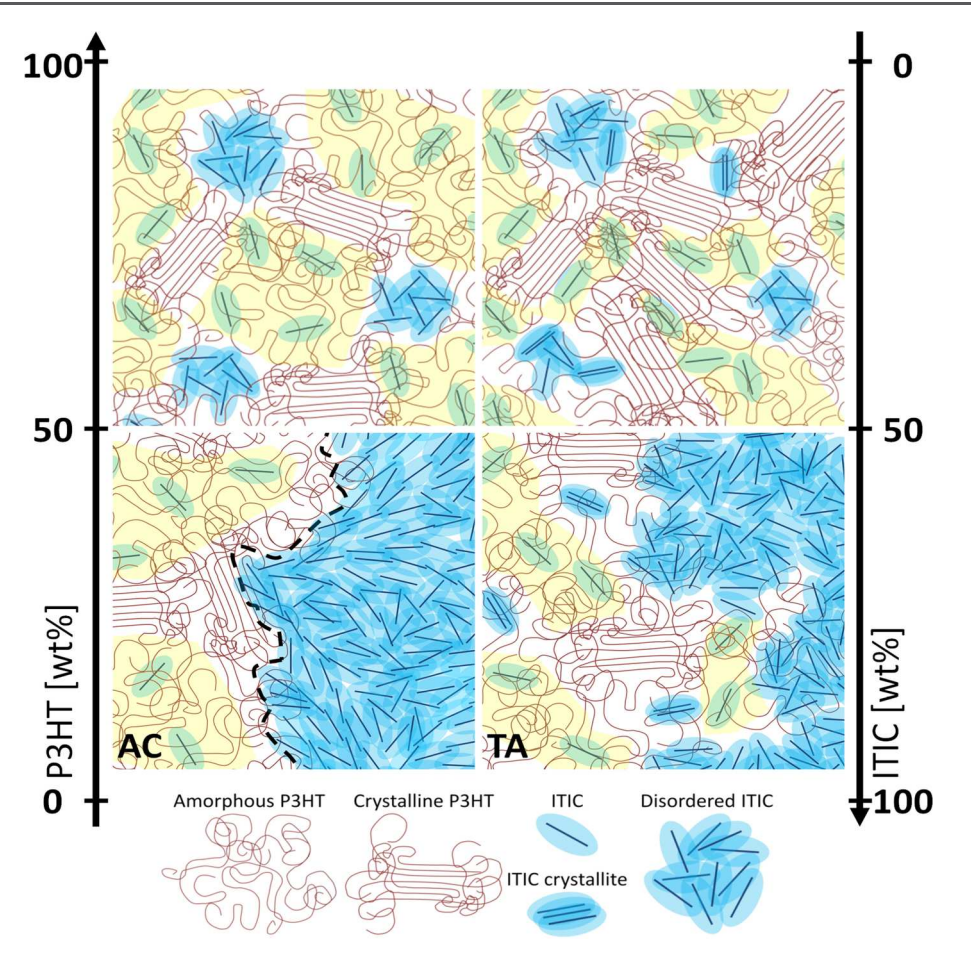


Figure 4. Schematic illustration of the morphology and microstructure of P3HT: ITIC blends as a function of composition (P3HT-rich in upper row, ITIC-rich in lower row) and processing conditions (AC left column and TA right column). The types of aggregates and domains present in the film are shown in the schematic legend below. The yellow background represents the intermixed glassy phase while the ITIC-rich glassy phase is represented by blue domains with non-oriented "molecules". The illustration shows that in P3HT-rich blends, both glassy phases are present as nanosized domains, evenly distributed in the BHJ. In contrast, the NFA-rich blends show clear, lateral phase separation between large (>500 nm) domains of the glassy phases and polymer-rich domains, with the domain boundaries slightly blurred after annealing.

lateral phase separation in AC and TA 50:50 and 30:70 P3HT: ITIC blends might be the result of a breakup of the transient wetting layer due to an interfacial instability during spin coating (spinodal decomposition), similar to that reported for BHJ polymer/polymer systems. <sup>49</sup> In agreement with this view, a high surface roughness is found for these samples that is significantly more pronounced compared to P3HT-rich blends which display a horizontal phase segregation. We also note that this type and the dimension of phase separation, in combination with the significant surface roughness explains the very low efficiencies of corresponding solar cells. <sup>30</sup>

In summary, we combined the insights gained by different materials characterization techniques to obtain mechanistic insights on the morphology and phase evolution of a prototypical polymer: NFA system. Different morphology regimes can be identified based on composition (P3HT-rich and ITIC-rich,) and processing conditions used (as-cast and after annealing at 150 °C), as schematically illustrated in Figure 4. The AC P3HT-rich films (top left) are composed of crystalline P3HT, domains of a glassy phase of intermixed P3HT: ITIC, and amorphous, relatively phase-pure (ITIC-rich) domains. The glassy domains are nanometer-sized and homogeneously dispersed in the polymer matrix (Figure 4, top left). When increasing the ITIC content modestly, larger glassy

domains are formed that generally accumulate at the bottom film surface; i.e., a vertical phase separation is observed. In contrast, AC films that are very ITIC-rich show a clear lateral phase separation of large glassy domains (both intermixed and ITIC-rich phases) separated by thinner P3HT-rich domains (Figure 4, bottom left). The boundaries between the glassy and P3HT-rich phases are distinct and the size of the P3HT-rich domains decreases with decreasing P3HT content. Upon annealing, in P3HT-rich films, the intermixed glassy domains phase separate, leading to an increase of the ITIC-rich amorphous fraction, that can crystallize upon further heating. Accordingly, a higher fraction and larger crystalline ITIC domains are formed at the expense of the intermixed glassy phase (Figure 4, top right), while, simultaneously, the degree of crystallinity of P3HT increases as well. For ITIC-rich samples, thermal annealing has a relatively small effect; only a blurring of the phase boundaries between the laterally separated domains is observed (bottom right).

Our work, hence, illustrates that the morphology of NFA-based BHJs can be highly complex. The coexistence of multiple glassy phases renders establishment of widely applicable processing/structure/performance interrelationships intricate. However, it may also provide opportunities because of the possibly highly diverse optoelectronic landscapes of such OSC

systems that may be accessed as a function of composition and processing. Understanding the morphology evolution of a polymer: NFA BHJ with composition and temperature could, therefore, provide a knowledge platform that will assist revealing the intricacy and complexity of such systems including multiple glassy phases and nontrivial macro-scale phase separation. Moreover, the composition of the amorphous intermixed phase may be estimated, especially if employing fast calorimetry.<sup>13</sup> Overall, our approach further advances the field via deeper insight of the phase behavior of complex blend systems.

#### ASSOCIATED CONTENT

### **Supporting Information**

The Supporting Information is available free of charge at https://pubs.acs.org/doi/10.1021/acsmaterialslett.2c00625.

Materials, sample preparation, characterization tools, methods, and supporting data and discussion, including GIWAXS plots and analysis, DSC thermal analysis, and HRSEM micrographs (PDF)

#### AUTHOR INFORMATION

#### **Corresponding Authors**

Gitti L. Frey — Department of Material Science and Engineering, Technion - Israel Institute of Technology, Haifa 3200003, Israel; oorcid.org/0000-0002-7638-4712; Email: gitti@technion.ac.il

Natalie Stingelin — School of Materials Science and Engineering, Georgia Institute of Technology, Atlanta, Georgia 30332, United States; Email: natalie.stingelin@gatech.edu

#### **Authors**

Oded Nahor — Department of Material Science and Engineering, Technion - Israel Institute of Technology, Haifa 3200003, Israel

Aditi Khirbat — School of Materials Science and Engineering, Georgia Institute of Technology, Atlanta, Georgia 30332, United States

Sebastian Alexander Schneider – Stanford Synchrotron Radiation Lightsource, SLAC National Accelerator Laboratory, Menlo Park, California 94025, United States; Department of Chemistry, Stanford University, Stanford, California 94305, United States

Michael F. Toney — Department of Chemical and Biological Engineering, University of Colorado, Boulder, Colorado 80309, United States; orcid.org/0000-0002-7513-1166

Complete contact information is available at: https://pubs.acs.org/10.1021/acsmaterialslett.2c00625

#### **Author Contributions**

CRediT: Oded Nahor data curation, formal analysis, investigation, methodology, writing-original draft; Aditi Khirbat data curation, formal analysis, investigation, methodology, writing-review & editing; Sebastian Schneider data curation, formal analysis, investigation, methodology, writing-review & editing; Michael F Toney formal analysis, funding acquisition, investigation, supervision, writing-review & editing; Natalie Stingelin conceptualization, formal analysis, funding acquisition, project administration, resources, supervision, writing-review & editing; Gitti L. Frey conceptualization, formal analysis, funding acquisition, investigation, investigation, investigation,

methodology, project administration, resources, supervision, writing-review & editing.

#### Notes

The authors declare no competing financial interest.

#### ACKNOWLEDGMENTS

This research was supported by a joint NSF-BSF grant via project #1905901 (NSF) and project #2018652 (BSF). M.F.T. and S.A.S. gratefully acknowledge support from the Department of the Navy, Office of Naval Research, Award No. N00014-21-1-2180.

#### REFERENCES

- (1) Andersen, T. R.; Dam, H. F.; Hösel, M.; Helgesen, M.; Carlé, J. E.; Larsen-Olsen, T. T.; Gevorgyan, S. A.; Andreasen, J. W.; Adams, J.; Li, N.; Machui, F.; Spyropoulos, G. D.; Ameri, T.; Lemaître, N.; Legros, M.; Scheel, A.; Gaiser, D.; Kreul, K.; Berny, S.; Lozman, O. R.; Nordman, S.; Välimäki, M.; Vilkman, M.; Søndergaard, R. R.; Jørgensen, M.; Brabec, C. J.; Krebs, F. C. Scalable, Ambient Atmosphere Roll-to-Roll Manufacture of Encapsulated Large Area, Flexible Organic Tandem Solar Cell Modules. *Energy Environ. Sci.* 2014, 7, 2925–2933.
- (2) Burgués-Ceballos, I.; Stella, M.; Lacharmoise, P.; Martínez-Ferrero, E. Towards Industrialization of Polymer Solar Cells: Material Processing for Upscaling. *J. Mater. Chem. A* **2014**, *2*, 17711–17722.
- (3) Carlé, J. E.; Helgesen, M.; Hagemann, O.; Hösel, M.; Heckler, I. M.; Bundgaard, E.; Gevorgyan, S. A.; Søndergaard, R. R.; Jørgensen, M.; García-Valverde, R.; Chaouki-Almagro, S.; Villarejo, J. A.; Krebs, F. C. Overcoming the Scaling Lag for Polymer Solar Cells. *Joule* 2017, 1, 274–289.
- (4) He, Z.; Zhong, C.; Su, S.; Xu, M.; Wu, H.; Cao, Y. Enhanced Power-Conversion Efficiency in Polymer Solar Cells Using an Inverted Device Structure. *Nat. Photonics* **2012**, *6*, 591–595.
- (5) Liu, Q.; Jiang, Y.; Jin, K.; Qin, J.; Xu, J.; Li, W.; Xiong, J.; Liu, J.; Xiao, Z.; Sun, K.; Yang, S.; Zhang, X.; Ding, L. 18% Efficiency Organic Solar Cells. *Sci. Bull.* **2020**, *65*, 272–275.
- (6) Hou, J.; Inganäs, O.; Friend, R. H.; Gao, F. Organic Solar Cells Based on Non-Fullerene Acceptors. *Nat. Mater.* **2018**, *17*, 119.
- (7) Armin, A.; Li, W.; Sandberg, O. J.; Xiao, Z.; Ding, L.; Nelson, J.; Neher, D.; Vandewal, K.; Shoaee, S.; Wang, T.; Ade, H.; Heumüller, T.; Brabec, C.; Meredith, P. A History and Perspective of Non-Fullerene Electron Acceptors for Organic Solar Cells. *Adv. Energy Mater.* **2021**, *11*, 2003570.
- (8) Yu, L.; Qian, D.; Marina, S.; Nugroho, F. A. A.; Sharma, A.; Hultmark, S.; Hofmann, A. I.; Kroon, R.; Benduhn, J.; Smilgies, D. M.; Vandewal, K.; Andersson, M. R.; Langhammer, C.; Martín, J.; Gao, F.; Müller, C. Diffusion-Limited Crystallization: A Rationale for the Thermal Stability of Non-Fullerene Solar Cells. *ACS Appl. Mater. Interfaces* **2019**, *11*, 21766–21774.
- (9) Marina, S.; Scaccabarozzi, A. D.; Gutierrez-Fernandez, E.; Solano, E.; Khirbat, A.; Ciammaruchi, L.; Iturrospe, A.; Balzer, A.; Yu, L.; Gabirondo, E.; Monnier, X.; Sardon, H.; Anthopoulos, T. D.; Caironi, M.; Campoy-Quiles, M.; Müller, C.; Cangialosi, D.; Stingelin, N.; Martin, J. Polymorphism in Non-Fullerene Acceptors Based on Indacenodithienothiophene. *Adv. Funct. Mater.* **2021**, *31*, 2103784.
- (10) Collins, B. A.; Gann, E.; Guignard, L.; He, X.; McNeill, C. R.; Ade, H. Molecular Miscibility of Polymer-Fullerene Blends. *J. Phys. Chem. Lett.* **2010**, *1*, 3160–3166.
- (11) Collins, B. A.; Li, Z.; Tumbleston, J. R.; Gann, E.; McNeill, C. R.; Ade, H. Absolute Measurement of Domain Composition and Nanoscale Size Distribution Explains Performance in PTB7:PC71BM Solar Cells. *Adv. Energy Mater.* **2013**, *3*, 65–74.
- (12) Zhao, J.; Li, Y.; Yang, G.; Jiang, K.; Lin, H.; Ade, H.; Ma, W.; Yan, H. Efficient Organic Solar Cells Processed from Hydrocarbon Solvents. *Nat. Energy* **2016**, *1*, 15027.
- (13) Marina, S.; Kaufmann, N. P.; Karki, A.; Gutiérrez-Meza, E.; Gutiérrez-Fernández, E.; Vollbrecht, J.; Solano, E.; Walker, B.;

- Bannock, J. H.; de Mello, J.; Silva, C.; Nguyen, T.; Cangialosi, D.; Stingelin, N.; Martín, J. The Importance of Quantifying the Composition of the Amorphous Intermixed Phase in Organic Solar Cells. *Adv. Mater.* **2020**, 32, 2005241.
- (14) Huang, Y.; Liu, X.; Wang, C.; Rogers, J. T.; Su, G. M.; Chabinyc, M. L.; Kramer, E. J.; Bazan, G. C. Structural Characterization of a Composition Tolerant Bulk Heterojunction Blend. *Adv. Energy Mater.* **2014**, *4*, 1301886.
- (15) Levitsky, A.; Matrone, G. M.; Khirbat, A.; Bargigia, I.; Chu, X.; Nahor, O.; Segal-Peretz, T.; Moulé, A. J.; Richter, L. J.; Silva, C.; Stingelin, N.; Frey, G. L. Toward Fast Screening of Organic Solar Cell Blends. *Adv. Sci.* **2020**, *7*, 2000960.
- (16) Liao, H. C.; Ho, C. C.; Chang, C. Y.; Jao, M. H.; Darling, S. B.; Su, W. F. Additives for Morphology Control in High-Efficiency Organic Solar Cells. *Mater. Today* **2013**, *16*, 326–336.
- (17) Huang, J.; Carpenter, J. H.; Li, C.-Z.; Yu, J.-S.; Ade, H.; Jen, A. K.-Y. Highly Efficient Organic Solar Cells with Improved Vertical Donor—Acceptor Compositional Gradient Via an Inverted Off-Center Spinning Method. *Adv. Mater.* **2016**, *28*, 967–974.
- (18) Deng, D.; Zhang, Y.; Zhang, J.; Wang, Z.; Zhu, L.; Fang, J.; Xia, B.; Wang, Z.; Lu, K.; Ma, W.; Wei, Z. Fluorination-Enabled Optimal Morphology Leads to over 11% Efficiency for Inverted Small-Molecule Organic Solar Cells. *Nat. Commun.* **2016**, *7*, 1–9.
- (19) Zhang, L.; Yi, N.; Zhou, W.; Yu, Z.; Liu, F.; Chen, Y. Miscibility Tuning for Optimizing Phase Separation and Vertical Distribution toward Highly Efficient Organic Solar Cells. *Adv. Sci.* **2019**, *6*, 1900565.
- (20) Westacott, P.; Tumbleston, J. R.; Shoaee, S.; Fearn, S.; Bannock, J. H.; Gilchrist, J. B.; Heutz, S.; Demello, J.; Heeney, M.; Ade, H.; Durrant, J.; McPhail, D. S.; Stingelin, N. On the Role of Intermixed Phases in Organic Photovoltaic Blends. *Energy Environ. Sci.* 2013, 6, 2756–2764.
- (21) Ye, L.; Hu, H.; Ghasemi, M.; Wang, T.; Collins, B. A.; Kim, J. H.; Jiang, K.; Carpenter, J. H.; Li, H.; Li, Z.; McAfee, T.; Zhao, J.; Chen, X.; Lai, J. L. Y.; Ma, T.; Bredas, J. L.; Yan, H.; Ade, H. Quantitative Relations between Interaction Parameter, Miscibility and Function in Organic Solar Cells. *Nat. Mater.* **2018**, *17*, 253–260.
- (22) Westacott, P.; Treat, N. D.; Martin, J.; Bannock, J. H.; de Mello, J. C.; Chabinyc, M.; Sieval, A. B.; Michels, J. J.; Stingelin, N. Origin of Fullerene-Induced Vitrification of Fullerene:Donor Polymer Photovoltaic Blends and Its Impact on Solar Cell Performance. *J. Mater. Chem. A* **2017**, *5*, 2689–2700.
- (23) Levitsky, A.; Schneider, S. A.; Rabkin, E.; Toney, M. F.; Frey, G. L. Bridging the Thermodynamics and Kinetics of Temperature-Induced Morphology Evolution in Polymer/Fullerene Organic Solar Cell Bulk Heterojunction. *Mater. Horizons* **2021**, *8*, 1272–1285.
- (24) Xin, J.; Meng, X.; Xu, X.; Zhu, Q.; Naveed, H. B.; Ma, W. Cold Crystallization Temperature Correlated Phase Separation, Performance, and Stability of Polymer Solar Cells. *Matter* **2019**, *1*, 1316–1330.
- (25) Wu, S.-C.; Strover, L. T.; Yao, X.; Chen, X.-Q.; Xiao, W.-J.; Liu, L.-N.; Wang, J.; Visoly-Fisher, I.; Katz, E. A.; Li, W.-S. UV-Cross-Linkable Donor—Acceptor Polymers Bearing a Photostable Conjugated Backbone for Efficient and Stable Organic Photovoltaics. ACS Appl. Mater. Interfaces 2018, 10, 35430—35440.
- (26) Ghasemi, M.; Hu, H.; Peng, Z.; Rech, J. J.; Angunawela, I.; Carpenter, J. H.; Stuard, S. J.; Wadsworth, A.; McCulloch, I.; You, W.; Ade, H. Delineation of Thermodynamic and Kinetic Factors That Control Stability in Non-Fullerene Organic Solar Cells. *Joule* **2019**, 3, 1328–1348.
- (27) Müller, C. On the Glass Transition of Polymer Semiconductors and Its Impact on Polymer Solar Cell Stability. *Chem. Mater.* **2015**, *27*, 2740–2754.
- (28) Yan, C.; Barlow, S.; Wang, Z.; Yan, H.; Jen, A. K. Y.; Marder, S. R.; Zhan, X. Non-Fullerene Acceptors for Organic Solar Cells. *Nat. Rev. Mater.* **2018**, *3*, 18003.
- (29) Lin, Y.; Wang, J.; Zhang, Z.-G.; Bai, H.; Li, Y.; Zhu, D.; Zhan, X. An Electron Acceptor Challenging Fullerenes for Efficient Polymer Solar Cells. *Adv. Mater.* **2015**, *27*, 1170–1174.

- (30) Qin, Y.; Uddin, M. A.; Chen, Y.; Jang, B.; Zhao, K.; Zheng, Z.; Yu, R.; Shin, T. J.; Woo, H. Y.; Hou, J. Highly Efficient Fullerene-Free Polymer Solar Cells Fabricated with Polythiophene Derivative. *Adv. Mater.* **2016**, 28, 9416–9422.
- (31) Müller, C.; Ferenczi, T. A. M.; Campoy-Quiles, M.; Frost, J. M.; Bradley, D. D. C.; Smith, P.; Stingelin-Stutzmann, N.; Nelson, J. Binary Organic Photovoltaic Blends: A Simple Rationale for Optimum Compositions. *Adv. Mater.* **2008**, *20*, 3510–3515.
- (32) Zhao, J.; Swinnen, A.; Van Assche, G.; Manca, J.; Vanderzande, D.; Mele, B. V. Phase Diagram of P3HT/PCBM Blends and Its Implication for the Stability of Morphology. *J. Phys. Chem. B* **2009**, *113*, 1587–1591.
- (33) Chen, D.; Nakahara, A.; Wei, D.; Nordlund, D.; Russell, T. P. P3HT/PCBM Bulk Heterojunction Organic Photovoltaics: Correlating Efficiency and Morphology. *Nano Lett.* **2011**, *11*, 561–567.
- (34) Hu, H.; Ghasemi, M.; Peng, Z.; Zhang, J.; Rech, J. J.; You, W.; Yan, H.; Ade, H. The Role of Demixing and Crystallization Kinetics on the Stability of Non-Fullerene Organic Solar Cells. *Adv. Mater.* **2020**, 32, 2005348.
- (35) Qu, Y.; Li, L.; Lu, G.; Zhou, X.; Su, Q.; Xu, W.; Li, S.; Zhang, J.; Yang, X. A Novel Melting Behavior of Poly(3-Alkylthiophene) Cocrystals: Premelting and Recrystallization of Component Polymers. *Polym. Chem.* **2012**, *3*, 3301–3307.
- (36) Snyder, C. R.; DeLongchamp, D. M. Glassy Phases in Organic Semiconductors. *Current Opinion in Solid State and Materials Science.* **2018**, 22, 41–48.
- (37) Mai, J.; Xiao, Y.; Zhou, G.; Wang, J.; Zhu, J.; Zhao, N.; Zhan, X.; Lu, X. Hidden Structure Ordering Along Backbone of Fused-Ring Electron Acceptors Enhanced by Ternary Bulk Heterojunction. *Adv. Mater.* **2018**, *30*, 1802888.
- (38) Treat, N. D.; Brady, M. A.; Smith, G.; Toney, M. F.; Kramer, E. J.; Hawker, C. J.; Chabinyc, M. L. Interdiffusion of PCBM and P3HT Reveals Miscibility in a Photovoltaically Active Blend. *Adv. Energy Mater.* **2011**, *1*, 82–89.
- (39) Verploegen, E.; Mondal, R.; Bettinger, C. J.; Sok, S.; Toney, M. F.; Bao, Z. Effects of Thermal Annealing Upon the Morphology of Polymer–Fullerene Blends. *Adv. Funct. Mater.* **2010**, *20*, 3519–3529.
- (40) Bartelt, J. A.; Beiley, Z. M.; Hoke, E. T.; Mateker, W. R.; Douglas, J. D.; Collins, B. A.; Tumbleston, J. R.; Graham, K. R.; Amassian, A.; Ade, H.; Fréchet, J. M. J.; Toney, M. F.; McGehee, M. D. The Importance of Fullerene Percolation in the Mixed Regions of Polymer–Fullerene Bulk Heterojunction Solar Cells. *Adv. Energy Mater.* **2013**, *3*, 364–374.
- (41) Oosterhout, S. D.; Savikhin, V.; Zhang, J.; Zhang, Y.; Burgers, M. A.; Marder, S. R.; Bazan, G. C.; Toney, M. F. Mixing Behavior in Small Molecule:Fullerene Organic Photovoltaics. *Chem. Mater.* **2017**, 29, 3062–3069.
- (42) Defour, M.; Van den Brande, N.; Van Lokeren, L.; Van Assche, G.; Maes, W.; Vanderzande, D.; Van Mele, B. Influence of the Amorphous Phase and Preceding Solution Processing on the Eutectic Behaviour in the State Diagram of P3HT: PC61BM Determined by Rapid Heat—Cool Calorimetry. *RSC Adv.* **2016**, *6*, 92981—92988.
- (43) Leng, C. Z.; Losego, M. D. Vapor Phase Infiltration (VPI) for Transforming Polymers into Organic–Inorganic Hybrid Materials: A Critical Review of Current Progress and Future Challenges. *Mater. Horizons* **2017**, *4*, 747–771.
- (44) Obuchovsky, S.; Shamieh, B.; Deckman, I.; Ankonina, G.; Frey, G. L. Harnessing ALD to Directly Map the Morphology of Organic Photovoltaic Bulk Heterojunctions. *Sol. Energy Mater. Sol. Cells* **2015**, 143, 280–283.
- (45) Obuchovsky, S.; Frankenstein, H.; Vinokur, J.; Hailey, A. K.; Loo, Y.-L.; Frey, G. L. Mechanism of Metal Oxide Deposition from Atomic Layer Deposition inside Nonreactive Polymer Matrices: Effects of Polymer Crystallinity and Temperature. *Chem. Mater.* **2016**, 28, 2668–2676.
- (46) Obuchovsky, S.; Levin, M.; Levitsky, A.; Frey, G. L. Morphology Visualization of P3HT:Fullerene Blends by Using Subsurface Atomic Layer Deposition. *Org. Electron.* **2017**, *49*, 234–241.

- (47) Chen, W.; Sun, Q. Q.; Xu, M.; Ding, S. J.; Zhang, D. W.; Wang, L. K. Atomic Layer Deposition of Hafnium Oxide from Tetrakis-(Ethylmethylamino) Hafnium and Water Precursors. *J. Phys. Chem. C* **2007**, *111*, 6495–6499.
- (48) Hausmann, D. M.; Kim, E.; Becker, J.; Gordon, R. G. Atomic Layer Deposition of Hafnium and Zirconium Oxides Using Metal Amide Precursors. *Chem. Mater.* **2002**, *14*, 4350–4358.
- (49) Heriot, S. Y.; Jones, R. A. L. An Interfacial Instability in a Transient Wetting Layer Leads to Lateral Phase Separation in Thin Spin-Cast Polymer-Blend Films. *Nat. Mater.* **2005**, *4*, 782–786.

## **□** Recommended by ACS

Volatile Solvent Additives Enabling High-Efficiency Organic Solar Cells without Thermal Annealing

Hui Lin, Silu Tao, et al.

DECEMBER 07, 2022

ACS APPLIED ENERGY MATERIALS

READ 🗹

Improving the Molecular Packing Order and Vertical Phase Separation of the P3HT:O-IDTBR Blend by Extending the Crystallization Period of O-IDTBR

Yadi Liu, Yanchun Han, et al.

SEPTEMBER 26, 2022

ACS APPLIED MATERIALS & INTERFACES

READ 🗹

Efficient and Thermally Stable Organic Solar Cells via a Fully Halogen-Free Active Blend and Solvent

Huan Zhao, Weijie Song, et al.

JANUARY 19, 2023

ACS APPLIED ENERGY MATERIALS

READ 🗹

**Tuning the Phase Separation by Thermal Annealing Enables High-Performance All-Small-Molecule Organic Solar Cells** 

Lingxian Meng, Yongsheng Chen, et al.

MARCH 22, 2022

CHEMISTRY OF MATERIALS

READ **C** 

Get More Suggestions >